

Chemical alloying and light-induced collapse of intermediate phases in chalcogenide glasses

Fei Wang^{1,4}, P Boolchand¹, K A Jackson² and M Micoulaut³

¹ Department of Electrical and Computer Engineering, University of Cincinnati, Cincinnati, OH 45221-0030, USA

² Department of Physics, Central Michigan University, Mt Pleasant, MI 48858, USA

³ Laboratoire de Physique Theorique des Liquides, Universite Pierre et Marie Curie, Boite 121 4, Place Jussieu, 75252 Paris Cedex 05, France

Received 11 December 2006, in final form 20 March 2007

Published 3 May 2007

Online at stacks.iop.org/JPhysCM/19/226201

Abstract

The elastic behaviour of binary $\text{Ge}_x\text{Se}_{1-x}$ glasses, examined in Raman scattering experiments earlier, has shown glasses at $x < 0.20$ to be in the flexible phase, those at $x > 0.25$ to be in the stressed-rigid phase and those in the $0.20 < x < 0.25$ range to be in the intermediate phase (IP). The IP width in mean-coordination-number space, $\Delta r = 0.10$. We have now examined ternary $\text{Ge}_{1/4}\text{Se}_{3/4-y}\text{I}_y$ glasses in Raman scattering and modulated DSC experiments, and find that the IP width dramatically collapses by an order of magnitude to $\Delta r = 0.009(2)$. Alloying iodine for Se serves to scission the network backbone progressively as mixed $\text{Ge}(\text{Se})_{4-m}\text{I}_m$ tetrahedra (m -units) emerge with $1 < m < 4$. The concentrations of various m -units are quantitatively tracked in Raman scattering, and this shows the $m = 1$ units to be rather special because they are isostatic. The present results on $\text{Ge}_{1/4}\text{Se}_{3/4-y}\text{I}_y$ glasses, when compared to those on $\text{Ge}_{1/4}\text{S}_{3/4-y}\text{I}_y$ glasses, reveal crucial differences in the way the reversibility window collapse occurs. Raman scattering examined as a function of the exciting light (647 nm) power (\mathcal{P}) in $\text{Ge}_{1/4}\text{Se}_{3/4-y}\text{I}_y$ glasses shows the IP to systematically collapse and to vanish once \mathcal{P} increases to $1.5 \times 10^6 \text{ W cm}^{-2}$. Here, an intense beam of near-bandgap light serves to optically pump the delicate intermediate range order prevailing in the IP and reversibly destroy it.

(Some figures in this article are in colour only in the electronic version)

1. Introduction

Stoichiometric GeS_2 and GeSe_2 [1–3] are known to exist in two crystalline polymorphs, a high temperature form (α), and a low temperature (β) form. The crystalline structures are composed

⁴ Present address: Department of Electrical Engineering, California Polytechnic State University, San Luis Obispo, CA 93407, USA.

of tetrahedral $\text{Ge}(\text{Se}_{1/2} \text{ or } \text{S}_{1/2})_4$ units that form a sheet-like (2D) morphology in the high temperature form and a 3D morphology in the low temperature form. The close similarities in crystalline structures suggest that replacement of Se by S serves merely to scale the underlying bond-lengths without changing the global morphology. Indeed, these ideas have also provided the inspiration to draw analogies in the glass forming tendencies and molecular structures of the binary $\text{Ge}_x\text{S}_{1-x}$ and $\text{Ge}_x\text{Se}_{1-x}$ glass systems. Thus, optimization of the glass forming tendency [4, 5] near $x \sim 20\%$ in these binary systems is broadly a reflection of the similarity of their molecular structures.

In spite of these parallels, there are striking differences as well in the physical behaviour of these two glass systems. Some of these differences are readily traced to the glass forming tendency of the base materials, elemental S and Se. Elemental Se is an excellent glass former and consists of polymeric chains of Se_n , with the result that one can form bulk $\text{Ge}_x\text{Se}_{1-x}$ glasses continuously all the way to $x \rightarrow 0$ (pure Se). Elemental S is not a good glass former, as it crystallizes into a molecular solid [6], composed of S_8 crowns. For this reason it is difficult to form homogeneous bulk $\text{Ge}_x\text{S}_{1-x}$ glasses, once $x < 0.10$ and approaches pure S. Such glasses demix into a glassy network of Ge-cross-linked S_n -chains, and a micro-crystalline S_8 -rich phase, with concentrations of the micro-crystalline phase steadily increasing at the expense of the glassy phase as $x \rightarrow 0$. The signature of these two phases is two endotherms observed in scanning calorimetric measurements [7, 8], one associated with the glass transition of the former phase, and a second endotherm associated with the opening of the S_8 rings into S_n chains at a temperature $T = T_\lambda \sim 150^\circ\text{C}$ in the latter phase.

The higher chemical stability of S_8 rings over polymeric S_n chains has other important consequences; the ageing behaviour of the sulfide glasses differs sharply from the selenide glasses. For example, when held at room temperature ($T < T_g$) for several months, S_n -chain fragments of a $\text{Ge}_{0.20}\text{S}_{0.80}$ glass network steadily transform into S_8 rings, an observation documented in both Raman scattering [9, 10] and calorimetric measurements. The chain to ring transformation serves to compact the glass, describing the ageing of these glasses. The corresponding selenide glass behaves quite differently because Se_8 rings are not so stable as Se_n chains, and the chain to ring transformation is significantly retarded. Then there are additional differences, particularly in the way strain is distributed in these two glassy systems. In binary $\text{Ge}_x\text{Se}_{1-x}$ glasses, network strain is expected to be *homogeneously* distributed because the sizes [11] of Ge ($r = 1.22 \text{ \AA}$) and Se (1.17 \AA) atoms are nearly the same. Such is not the case in binary $\text{Ge}_x\text{S}_{1-x}$ glasses, where network strain is inhomogeneously distributed because of an *atomic size mismatch* between Ge ($r = 1.22 \text{ \AA}$) and S (1.02 \AA).

Indeed, these strain related ideas were recently confirmed in Raman experiments [11] using diamond anvil cells, where a blue-shift in the symmetric stretch mode of GeS_4 as a function of an externally applied pressure revealed quite different chemical trends from those of the symmetric stretch mode of GeSe_4 tetrahedra in corresponding selenide glasses.

The measurement of internal strain in network glasses poses formidable challenges. The issue was addressed theoretically by several groups [12] but with little advancement in basic understanding, largely because of the absence of crucial experimental results in the field. Recently, an important advance in the experiments came from pressure Raman experiments on binary $\text{Ge}_x\text{Se}_{1-x}$ glasses [11]. These show that in equi-atomic-size glassy networks strain is also determined by network connectivity (r). Wang *et al* showed that that under-coordinated ($r < 2.40$) and over-coordinated ($r > 2.40$) networks are, in general, stressed, while optimally coordinated ($r = 2.40$) networks form stress-free structures. The magic value of $r = 2.40$ for 3D networks is a mean-field condition that matches Lagrangian constraints due to bond-stretching and bond-bending forces per atom with the three available positional degrees of freedom/atom [4].

In this work, we take a new experimental approach to address the issue of stress in these binary Ge–Se and Ge–S glasses. We start with a fixed base glass composition, such as $\text{Ge}_{0.25}\text{Se}_{0.75}$, that is mildly stressed–rigid [5], and steadily replace Se atoms by I atoms. One expects large stress to accumulate around the tetrahedrally coordinated Ge atoms as the oversized I ($r = 1.33 \text{ \AA}$) atoms replace one or more of the Se ($r = 1.17 \text{ \AA}$) near neighbours to form mixed tetrahedral units $\text{Ge}(\text{Se})_{4-n}\text{I}_n$. On the other hand, in the corresponding sulfide glasses, a *size compensation effect* will come into play because S ($r = 1.02 \text{ \AA}$) has a much smaller size than I ($r = 1.33 \text{ \AA}$), and one does not expect stress around tetrahedrally coordinated Ge sites to increase until the average anion size (sulfur and iodine) exceeds that of Ge, a point we will return to later.

Iodine alloying in base $\text{Ge}_{0.25}\text{Se}_{0.75}$ glasses has another profound consequence; it lowers the network connectedness (r) as twofold coordinated Se or S atoms are replaced by onefold coordinated iodine atoms. Within mean-field constraint theory, the stressed–rigid to flexible elastic phase transition is predicted [13] to occur when the iodine concentration (y) increases to a critical value $y_c = 1/6$. Theory makes no distinction between S or Se, and in fact treats them as point objects. In practice, these atoms occupy a finite volume and lead to accumulation of stress in networks because of packing considerations. Thus, examination of ternary $\text{Ge}_{0.25}\text{Se}_{0.75-y}\text{I}_y$ glasses as a function of iodine content permits probing the role of *network stress* and *space-filling* in the nature of the *stressed–rigid to floppy* elastic phase transition.

In this work we report on the stressed–rigid to flexible elastic phase transition in $\text{Ge}_{0.25}\text{Se}_{0.75-y}\text{I}_y$ glasses for the first time. We find the transition to occur near $y_c \sim 1/6$, and to be rather *broad*. Close examination of the *broad transition* reveals that there are in fact *two closely spaced transitions and not one*. These two transitions serve to define a narrow intervening region, an *intermediate phase* (IP) [14–16]. The elastic phase transition in ternary $\text{Ge}_{0.25}\text{S}_{0.75-y}\text{I}_y$ sulfide glasses was examined earlier [13], and experiments placed the elastic phase boundary also near $y_c \sim 1/6$, but the transition was found to be surprisingly *sharp*. Thus, differences in onset of network flexibility in the ternary-selenide versus ternary-sulfide glasses provide important clues on atom-size-related accumulation of stress and in what manner this stress is dissipated when networks reconfigure in the IPs. The discovery of IPs in glasses has provided new insights into understanding [17–20] how disordered networks globally restructure themselves to lower their free energy by minimizing network stress. The aim of the present work is to understand the manner in which factors such as atomic size distribution and network connectivity come into play in IPs as networks self-organize. The present Raman scattering experiments, performed as a function of increasing laser power density, confirm that the IP in the ternary selenide glasses collapses at high power densities. The observation is in harmony with a previous observation of a collapse of the IP in binary $\text{Ge}_x\text{Se}_{1-x}$ glasses [5].

The remainder of this paper is organized as follows. After presenting the experimental results in section 2, we provide some theoretical background in section 3 to analyse the experimental data. The central structure results on the IP collapse by chemical alloying and separately by exposure to high power densities of light radiation are discussed in section 4. Conclusions are summarized in section 5.

2. Experimental details

2.1. Sample synthesis

Ternary $\text{Ge}_{25}\text{Se}_{75-y}\text{I}_y$ glasses were prepared by reacting 99.999% elemental germanium, selenium and GeI_4 as starting materials from Cerac Inc. GeI_4 melts at 144°C and exhibit significant vapour pressure at room temperature. The starting materials were handled in a dry nitrogen ambient. In vacuum sealing the starting materials, care was taken to cool the

mixture of starting materials to minimize loss of GeI_4 . Fused silica tubes containing the starting materials were immersed in a liquid nitrogen bath while pumping with a high vacuum system ($<10^{-7}$ Torr) to encapsulate samples in vacuum. Typical sample size was kept near 2 g to permit a reliable control on chemical composition of glasses, particularly of iodine (to about 1/10 of an atomic %). Sealed ampoules were slowly heated to 900 °C and then homogenized by holding at that temperature for at least 48 h. Melt temperatures were then slowly lowered to 30 °C above liquidus and kept there for 12 h before a water quench to realize bubble-free homogeneous bulk glasses. High iodine content samples ($y > 0.10$) generally required heating the starting materials at an extremely slow heating rate of 0.5 °C min^{-1} to avoid explosions. Homogeneity of glasses was investigated by Raman scattering without opening ampoules. When the observed Raman lineshapes along the length of the quartz tubes appeared to be the same, samples were taken to be homogeneous.

2.2. Temperature modulated differential scanning calorimetry

A model 2920 temperature modulating DSC (MDSC) from TA Instruments was used to establish glass transition properties. All scans used a 3 °C min^{-1} scan rate and a 1 °C/100 s modulation rate. Furthermore, each scan was initiated at a temperature about 50 °C below T_g , and the sample heated to 50 °C above T_g followed by a cool down cycle across T_g to the starting temperature. In MDSC, the total heat-flow response is deconvoluted into a reversing and a non-reversing heat-flow component [21]. The reversing heat-flow signal is that part of the total heat-flow signal that tracks the sinusoidal temperature variations. The deconvolution of the total heat flow into its two components has proved to be useful [22]; the reversing heat-flow signal relates to ergodic processes (thermodynamics) surrounding T_g , while the non-reversing heat-flow signal to the configurational changes accompanying structural arrest including ageing connected with T_g . The glass transition temperature (T_g) is deduced from the inflexion point of the reversing heat flow [23]. The area under the non-reversing enthalpy associated with T_g was obtained by integrating the signal going up in temperature, and then subtracting the corresponding signal coming down in temperature. This procedure yields the frequency-corrected non-reversing enthalpy (ΔH_{nr}) [21] associated with T_g . Figure 1 provides an MDSC scan of a ternary $\text{Ge}_{25}\text{Se}_{75-y}\text{I}_y$ glass at $y = 6\%$, with the total, reversing and non-reversing heat flow signals shown. The deduced thermal parameters, T_g and $\Delta H_{nr}(x)$, for the scan are also labelled. At each glass composition we measured three independent samples from a given batch to ascertain reproducibility of the thermal data. These data reveal the typical uncertainty in T_g to be 2 °C, and that in $\Delta H_{nr}(x)$ to be 1×10^{-5} J kg^{-1} .

Figure 2 provides a summary [11] of the variations in $T_g(x)$ and $\Delta H_{nr}(x)$ in binary $\text{Ge}_x\text{Se}_{1-x}$ glasses. ΔH_{nr} shows a global minimum in the $0.20 < x < 0.25$ range, and the term rapidly increases, once the Ge concentration $x > 0.25$, or $x < 0.20$. Figure 3 shows variations in T_g as a function of iodine content y in both ternary selenide and sulfide glasses. One observes $T_g(y)$ to systematically decrease as y increases. T_g reduction is at first slow, but then precipitous as y increases to a critical value, $y_c = 1/6$, in both ternary glasses. A summary of the variations in ΔH_{nr} for the Ge–Se–I ternary appears in figure 4. One observes a global minimum in ΔH_{nr} centred near $y_c \sim 1/6$, with the reversibility window being almost square-well-like. Compositional variations in T_g in binary and ternary glasses have been modelled and will be discussed in sections 3.3 and 4.2.2.

2.3. Raman scattering

Raman scattering was excited in a back-scattering configuration with samples wetting the quartz ampoules used to synthesize them. About 2 mW of 647.1 nm radiation from a Kr-

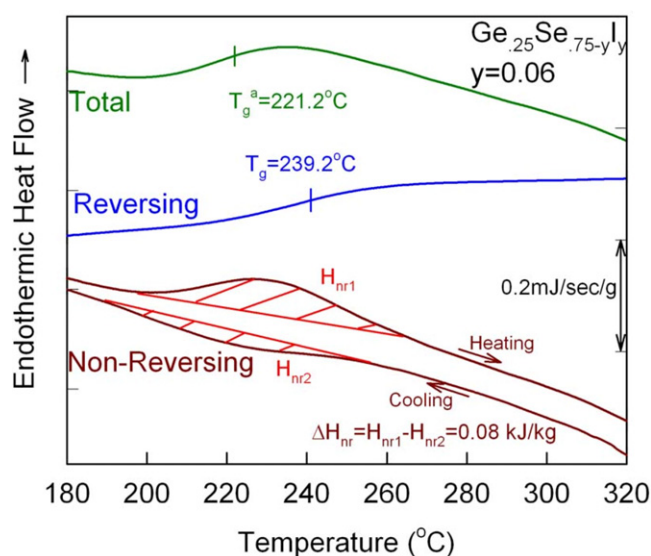


Figure 1. MDSC scan of the ternary $\text{Ge}_{0.25}\text{Se}_{0.75-y}\text{I}_y$ glass at $y = 0.06$ taken at 3°C min^{-1} scan rate and $1^\circ\text{C}/100\text{ s}$ modulation rate. The glass transition, deduced from the inflection point of the reversing heat flow, is $T_g = 239.2^\circ\text{C}$. The frequency-corrected non-reversing enthalpy, ΔH_{nr} , is obtained by subtracting the term ΔH_{nr2} (hatched area) obtained upon cooling from the term ΔH_{nr1} obtained upon heating. The apparent T_g^a deduced from the inflection point of the total heat flow is 221.2°C .

ion laser, focused to a $50\ \mu\text{m}$ spot size, was brought to a line focus on the inner surface of a cylindrical quartz ampoules containing a sample. The scattered light was analysed using a model T64000 triple monochromatic system [9] from Horiba-Jobin Yvon using a CCD detector. Figure 5 shows selected lineshapes in ternary $\text{Ge}_{1/4}\text{Se}_{3/4-y}\text{I}_y$ glasses. In the base glass ($y = 0$), one observes modes of corner sharing (CS) and edge sharing (ES) $\text{Ge}(\text{Se}_{1/2})_4$ tetrahedra as labelled [9]. The broad peak in the $240\text{--}270\ \text{cm}^{-1}$ range is due to the selenium chain mode (CM). Progressive iodine alloying produces new features (see arrows) at 185 , 170 , 168 and $155\ \text{cm}^{-1}$. These modes are identified as those of mixed $\text{Ge}(\text{Se}_{1/2})_{4-m}(\text{I})_m$ tetrahedra (m -units), having $m = 1, 2, 3$ and 4 iodine near neighbours (figure 6) respectively. The mixed-tetrahedron identification is supported by first principles cluster calculations and will be discussed in section 3.4.

Raman line-shapes were analysed in terms of a superposition of Gaussian peaks. Figure 7 illustrates an example of an observed lineshape that was analysed as a superposition of several Gaussian profiles with no restrictions on centroid, full width at half maximum or integrated intensity using a non-linear least squares fitting routine. Concentrations of m -units were then deduced from integrated intensity or scattering strength of each peak by folding in the calculated Raman cross-sections. Details of the Raman cross-section calculations are presented in section 3.4. Figure 8 shows the m -unit concentrations, $N(m, y)$, as a function of iodine content for the $\text{Ge}_{1/4}\text{Se}_{3/4-y}\text{I}_y$ ternary. The observed trends in concentrations show the following. (i) The $m = 1\text{--}4$ units broadly increase (coloured points and thick lines) at the expense of the $m = 0$ unit (black dots and thick line). The increase roughly follows the combinatorial predictions (black and coloured thin lines) for ternary sulfides [13] but such is not the case in ternary selenides. These predictions describe the expected variation of m -units when iodine *stochastically* replaces available bridging chalcogen sites in the backbone. (ii) A sharp

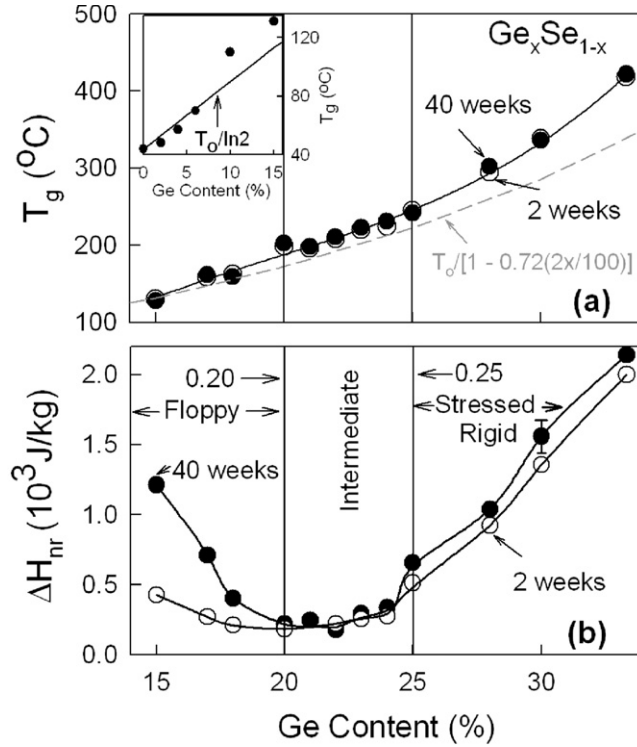


Figure 2. T -modulated DSC results on $\text{Ge}_x\text{Se}_{1-x}$ glasses showing variations in (a) $T_g(x)$ and (b) the non-reversing enthalpy $\Delta H_{nr}(x)$ measured 2 weeks (O) and 40 weeks (●) after synthesis. $T_g(x)$ increase monotonically with x and reveal no ageing effect. The ΔH_{nr} term shows a global minimum in the $0.20 < x < 0.25$ range (reversibility window), and the term increases both above ($x > 0.25$) and below ($x < 0.20$). The ΔH_{nr} term ages outside the reversibility window but ageing is qualitatively suppressed in the window. See the text for details. The dashed line in (a) gives the variations in T_g predicted using Lamb–Mossbauer factors and Lindemann’s melting criteria developed by Naumis [45]. The inset of (a) compares observed T_g values at low Ge concentrations taken from [58] with the SAT prediction (equation (3)), shown as a continuous line. At $x > 0.10$, a deviation between theory and experiment sets in as edge-sharing GeSe_2 tetrahedra emerge in binary glasses, and the agglomeration ceases to be strictly stochastic.

step in $N(1, y)$, the concentration of $m = 1$ units, is observed to start at $y_c(1) = 0.155(1)$ and end at $y_c(2) = 0.163(1)$. The location of the step as a function of y is found to coincide with the sharply defined reversibility window as shown in figure 9(a). (iii) The step is not observed in the ternary sulfide glasses [13], although we observe a mild kink in the concentration of $m = 3$ units which coincides with the onset of the reversibility window as shown in figure 9(b). (iv) In the selenide glasses, the concentration of $m = 1$ units is higher while that of $m = 0$ units lower than the combinatorial predictions over a wide range of iodine concentration. (v) Finally, the scattering strength ratio of CS to ES modes in ternary selenides is found to steadily decrease with iodine concentration in the $0 < y < 0.15$ range, and to show a rather sharply defined peak centred in the reversibility window as shown in figure 10. In this figure, the scattering strength ratio of CS to ES tetrahedra shows a peak value of about 3.0, nearly the same value as found in the pristine base $\text{Ge}_{25}\text{Se}_{75}$ glass [5]. These findings relate to structural changes taking place as the network self-organizes in the reversibility window, an issue we will discuss in section 4.

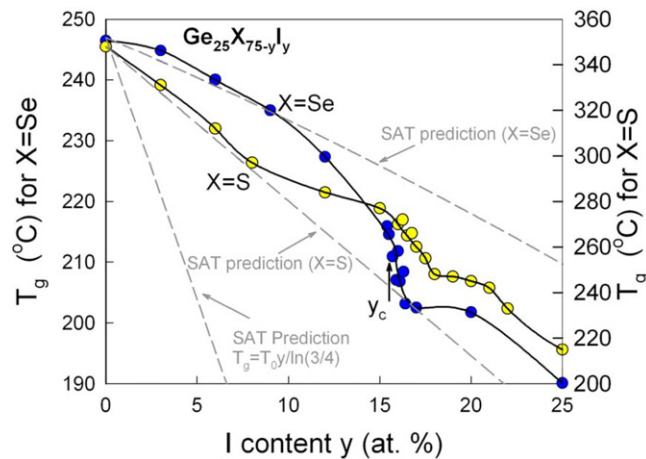


Figure 3. MDSC results on ternary $\text{Ge}_{25}\text{X}_{75-y}\text{I}_y$ glasses, $\text{X} = \text{Se}$ (●) and S (●), showing variations in T_g as a function of iodine content y . For $\text{X} = \text{Se}$ see the ordinate on the left while for $\text{X} = \text{S}$ see the ordinate on the right. T_g values in both ternaries decrease with iodine content y , and drop precipitously near $y \sim 1/6$. The SAT predictions for $T_g(y)$ are shown as broken lines. The third curve is a plot of equation (4). See the text for details and reference.

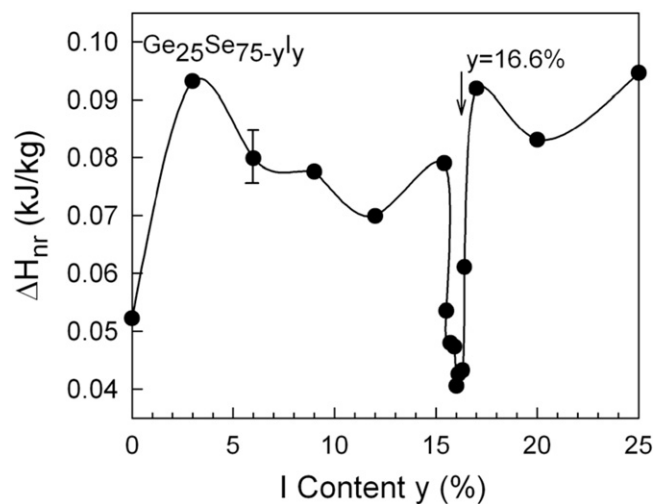


Figure 4. Variation in the non-reversing enthalpy, $\Delta H_{nr}(y)$, in the $\text{Ge}_{25}\text{Se}_{75-y}\text{I}_y$ ternary. The arrow locates ($y = 16.6\%$) the mean field rigidity transition. See the text for details.

2.4. Raman scattering as a function of laser light power

To examine light-induced effects on chalcogenide glasses, the T64000 Raman system was used in a micro-mode configuration. Radiation (647 nm) from a Kr-ion laser was brought to a tight focus of about $1 \mu\text{m}$ spot size using an Olympus BX41 microscope attachment. This has the consequence to increase the exciting light power density on a sample by at least three orders of magnitude. The samples, encapsulated in evacuated fused quartz tubing, had wetted the inner surfaces of tubes. Laser light was brought to a focus on the sample surface in contact

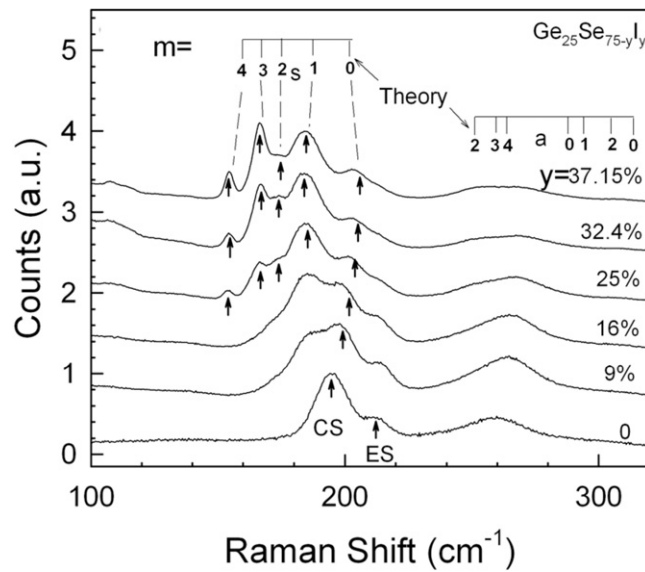


Figure 5. Room temperature Raman scattering in ternary $\text{Ge}_{25}\text{Se}_{75-y}\text{I}_y$ glasses at indicated iodine concentrations y . The arrows identify modes of the mixed tetrahedra, $\text{Ge}(\text{Se}_{1/2})_{4-m}\text{I}_m$, for various $m = 0, 1, 2, 3$ and 4 units. The bar chart on top gives predicted mode frequencies of the m -units based on cluster calculations. CS = corner sharing or A_1 , ES = edge sharing, s = symmetric and a = asymmetric mode.

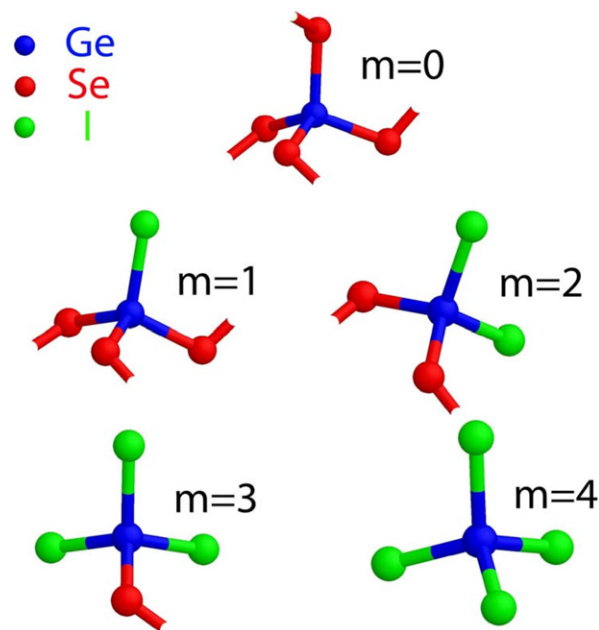


Figure 6. Schematic view of the molecular structure of various m -units. Here m indicates the number of iodine near neighbours of Ge. Blue = germanium atoms, red = selenium atoms and green = iodine atoms.

with quartz tubing using an $80\times$ objective. Back-scattered radiation was analysed using the triple subtractive mode. In these experiments laser light power on the sample was varied in the

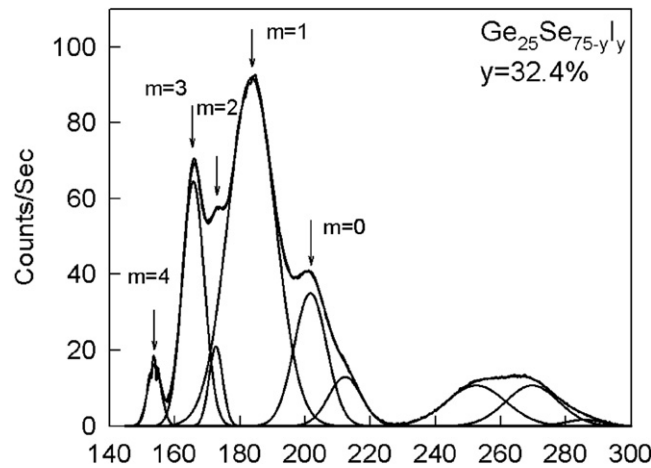


Figure 7. An example of a non-linear least squares fitting of the observed Raman lineshape of the title ternary selenide glass in terms of the requisite number of Gaussian lineshapes with no restrictions on the lineshape parameters: centroid, intensity or linewidth. The integrated intensities of the various modes were extracted and normalized to the scattering cross-sections to infer m -unit concentrations. See the text for details.

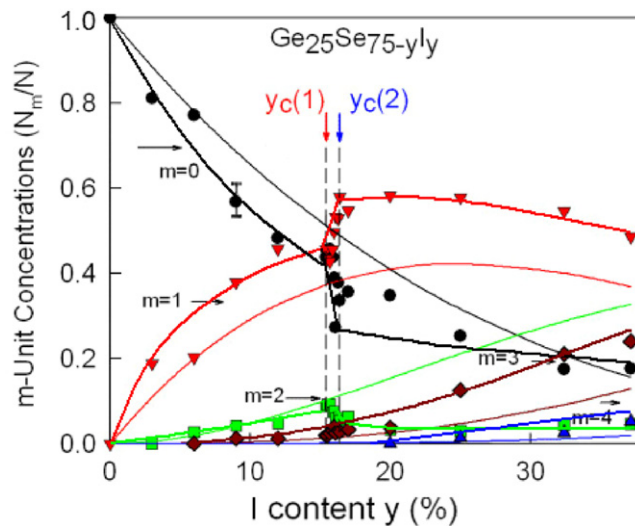


Figure 8. Variation in the concentrations of various m -units in ternary $\text{Ge}_{25}\text{Se}_{75-y}\text{I}_y$ glasses. Note the presence of a step in N_1/N and N_0/N . The colour codes are $m = 0$ black, $m = 1$ red, $m = 2$ green, $m = 3$ brown and $m = 4$ blue. The thick lines are smooth curves through the data points. The thin lines are results of combinatorial predictions. The reversibility windows extend in the $y_c(1) < y < y_c(2)$ range.

1 mW < \mathcal{P} < 15 mW range. These experiments were performed on ternary glass samples containing iodine in the 15.4% < y < 17% range. Upon increasing the laser power \mathcal{P} , the step-like increase in the concentration of the $m = 1$ units was steadily erased, as illustrated in figure 12. We will return to discuss these results in section 4.3.

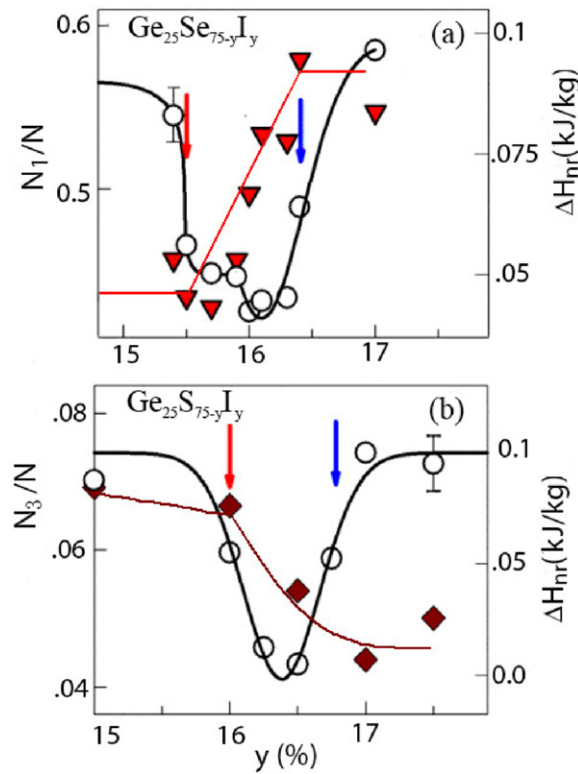


Figure 9. An enlarged view of the reversibility window in ternary (a) $\text{Ge}_{25}\text{Se}_{75-y}\text{I}_y$ and (b) $\text{Ge}_{25}\text{S}_{75-y}\text{I}_y$ glasses [13]. The open circles represent the non-reversing enthalpy, ΔH_{nr} . In (a) the filled triangles represent the normalized Raman scattering strength of $m = 1$ units, N_1/N . It displays a linear step starting at $y_c(1) = 0.155(1)$, and ending at $y_c(2) = 0.164(1)$, that coincides with the reversibility window walls. In (b) the $m = 3$ unit concentrations (N_3/N), represented by filled diamonds, show a mild kink near $y_c(1)$.

3. Theoretical

3.1. Stochastic networks and m -unit concentrations from combinatorics

One can predict the concentrations of the various m -units, $N_m(y)/N$, as a function of iodine content y , if iodine were to stochastically [13] replace bridging Se sites in the base $\text{Ge}_{25}\text{Se}_{75}$ glass. There are five possible local structures, $\text{Ge}(\text{S}_{1/2})_{4-m}\text{I}_m$, that can be populated (figure 6) in these glasses with $m = 0, 1, 2, 3$ and 4 , representing the number of iodine near neighbours of the tetrahedrally coordinated Ge atom. Thus, the probability of having m -units present in a glass of $\text{Ge}_{0.25}\text{Se}_{0.75-y}\text{I}_y$ composition is

$$P(m, y) = \frac{4!}{m!(4-m)!} y^m (1-y)^{4-m} \quad (0 \leq m \leq 4, 0 \leq y \leq 1). \quad (1)$$

The thin solid lines in figure 8 represent a plot of equation (1) for $m = 1, 2, 3$ and 4 . As expected, only $m = 0$ units prevail at $y = 0$ when the glasses are populated by GeSe_4 units. With increasing iodine content, $m = 0$ units are first converted to $m = 1$ units, and some of these $m = 1$ units are then converted to $m = 2$ units, and with the process ongoing to populate higher m -units as y increases. In particular, the calculations reveal $m = 4$ units to be first populated once y approximately exceeds 0.10.

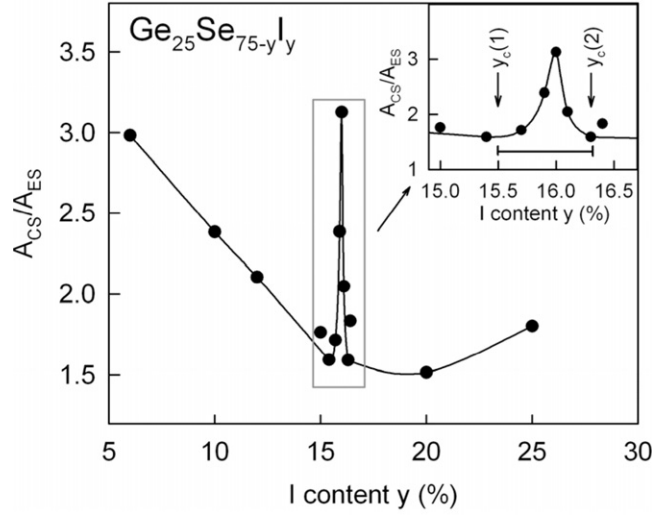


Figure 10. Variations in the ratio of corner sharing to edge sharing $m = 0$ tetrahedra in ternary $\text{Ge}_{25}\text{Se}_{75-y}\text{I}_y$ glasses showing a maximum near the centroid, $y = 0.160$, of the reversibility window. See the inset.

3.2. Lagrangian constraints of m -units

Bond-bending forces and bond-stretching ones serve as Lagrangian constraints in assembling covalent glassy networks. The count of Lagrangian constraints for various m -units (figure 6) can now be enumerated. We take the coordination number of Ge, Se and I to be $r = 4, 2$ and 1 respectively. In 3D, for an atom possessing a coordination number r , there are $r/2$ bond-stretching and $2r-3$ bond-bending constraints [24] provided r is equal to or greater than two. Onefold coordinated atoms have to be treated differently [25, 26] because one can only associate a bond-stretching force (constraint) with a terminal atom. Accordingly, we take half the constraint associated with an atom of coordination $r = 1$. For a $\text{Ge}(\text{S}_{1/2})_{4-m}\text{I}_m$ formula unit, we then obtain a total of seven constraints for Ge, two for Se or S and one-half for each iodine atom, yielding

$$n_c = [7 + 2(4 - m)/2 + m/2]/[1 + (4 - m)/2 + m] \quad (2a)$$

that may be re-written as,

$$n_c = \frac{[7 + (4 - m) + \frac{m}{2}]}{(3 + \frac{m}{2})} \quad (0 \leq m \leq 4). \quad (2b)$$

From equation (2b), we find that $n_c = 3.67, 3.00, 2.50$ and 2.11 respectively for $m = 0, 1, 2, 3$ and 4 units as summarized in table 1. The count highlights the special role of the $m = 1$ units that take on a value of three; i.e., these units are *optimally constrained* or *isostatic* in nature. On the other hand, the $m = 0$ units are *stressed-rigid* while the higher m -units, i.e. 2 and 3, are mechanically under-constrained as the number of dangling ends increase. The $m = 4$ units are totally decoupled from the network backbone and are thought to exist as isolated molecules in the glasses.

Table 1. Local $\text{Ge}((\text{Se or S})_{1/2})_{4-m}\text{I}_m$ local structures, their count of constraints per atom n_c and their mean coordination number $\langle r \rangle$.

Local structure	n_c	$\langle r \rangle$
$m = 0$	3.67 ^a	2.67 ^a
	3.00 ^b	2.40 ^b
$m = 1$	3.00	2.14
$m = 2$	2.50	1.75
$m = 3$	2.11	1.44
$m = 4$	1.80	1.40

^a For $\text{Ge}(\text{Se}_{1/2})_4$ tetrahedra bridging across Se atoms.^b For $\text{Ge}(\text{Se}_{1/2})_4$ tetrahedra bridging across Se–Se atoms.

3.3. Stochastic agglomeration theory and variations of $T_g(y)$ in chalcogenides

Relationships between glass transition temperature, T_g , and physical properties of glasses have been proposed in the past [27–29]. However, none of these approaches have been as successful as the topology based ones [30, 31]. In the latter, one considers agglomeration of local structural units to be driven by compositional changes, and variations in T_g are related to connectivity of glass structure. Stochastic agglomeration theory (SAT) [30, 31] provides a quantitative prediction for T_g if agglomeration of local structures proceeds in a stochastic or random fashion. The central idea is that one relates increase in viscosity of a glass-forming liquid as temperature decreases to the creation of covalent bonds between well defined local structures (LSs). Concentrations of LSs increase with time and temperature during discrete agglomeration steps as structural arrest occurs near T_g , and a stationary state evolves. The concentrations or probabilities of LSs then saturate, and solutions of master equations [31] describing the underlying agglomeration process take on constant values. The approach permits one to relate T_g to probabilities of occurrence of different LSs, and thus to the macroscopic modifier concentrations such as Ge atomic content in binary $\text{Ge}_x\text{Se}_{1-x}$ glasses or iodine atomic content in the present ternary glasses (see below).

In binary $\text{Ge}_x\text{Se}_{1-x}$ glasses, at low x (<0.20), Ge atoms *randomly* cross-link polymeric chains of Se_n . Under these circumstances, variations in T_g with x can be computed exactly using SAT [31], and one finds the slope to be given by a parameter-free relation,

$$dT_g/dx = T_0(x=0)/\ln(r_{\text{Ge}}/r_{\text{Se}}) \quad (3)$$

where r_{Ge} ($=4$) and r_{Se} ($=2$) denote the coordination numbers of Ge and Se respectively. The addition of higher coordinated Ge atoms to the base network of selenium chains steadily increases T_g in an almost linear fashion. The agreement between experiment (figure 2) and the SAT prediction (equation (3)) in binary $\text{Ge}_x\text{Se}_{1-x}$ glasses as well as in other network glasses [14, 32, 33] is excellent. At higher x (>0.20), the stochastic agglomeration process ceases to be stochastic as isostatically rigid local structures form and self-organize. At still higher x (>0.27) stressed–rigid corner-sharing $\text{Ge}(\text{Se}_{1/2})_4$ tetrahedra and homopolar Ge–Ge bonds form, and one does not expect SAT to really work. A comparison of theory with experiment (figure 2) clearly supports the general picture. Recently, a new theoretical approach [34] based on concepts of rigidity and Lindemann’s melting criterion [35–37] has been used to predict compositional trends of T_g in binary $\text{Ge}_x\text{Se}_{1-x}$ glasses. The predictions of this approach are in remarkably good accord with the results of SAT described above.

In the present ternary glasses the addition of iodine to the base glass ($m = 0$ units) lowers the connectedness of the network as $m = 1$ units are created. Topologically, six closed rings emanate from each Ge atom in an $m = 0$ unit but only three rings in the case of an $m = 1$ unit. Here the number of rings represents the number of ways one picks two branches out of a total

of four (for $m = 0$) or three (for $m = 1$). For the SAT calculations the minimalist choice of LSs is to consider $m = 0$ and 1 units, and the possible agglomerations will then include m -unit pairings such as 0–0, 0–1 and 1–1. If one simplifies the problem further by assuming that there are no correlations between the m -units, then the SAT-based slope equations predict [31]

$$dT_g/dy = T_g(y = 0)/\ln(3/4) \quad (4)$$

where the factor $\ln(3/4)$ results from growth of $m = 1$ units from $m = 0$ units. Similar ideas have been invoked to understand the sharp reduction of T_g when traces of soda (Na_2O) are added to a base SiO_2 glass network, and Q^3 units emerge at the expense of Q^4 ones with formation of non-bridging oxygen [38]. Equation (4) captures the zeroth order behaviour of $T_g(y)$ for the present ternary glasses (figure 3). A large change in connectivity can be expected to result in a steeper variation of T_g .

While this kind of SAT application is usually quite accurate [39] in simple binary chalcogenides or even oxide glasses, it appears here that equation (4) is not accurate enough (broken line in figure 2) to describe the observed $T_g(y)$ variation in the present ternary glasses. There are several reasons, and we shall visit the issues in section 4.2.2.

3.4. Density functional calculations of IR and Raman active mode frequencies, and cross-sections

First-principles calculations based on the local density approximation (LDA) were carried out to investigate the sharp peaks seen in the Raman spectra of figure 5. The calculations made use of a mixed pseudopotential/all-electron formalism [40, 41] implemented in the NRLMOL code [40]. Extensive, Gaussian orbital basis sets were used for all atoms in all the calculations. The cluster models shown in figure 6 were studied to systematically investigate $\text{GeX}_{(4-m)}\text{I}_m$ tetrahedra ($X = \text{S}$ or Se), with $m = 0, 1, 2, 3$ and 4. H-atoms (not shown in figure 6) were used to terminate dangling bonds so that all the X atoms in the models were twofold coordinated. Each cluster model was first relaxed to its minimum energy geometry. The full vibrational spectrum was then calculated in the harmonic approximation using a standard, finite-difference approach for building the force-constant matrix [42]. Finally, the Raman activities were computed for each vibrational mode, using a finite-field method that has been described in detail elsewhere [42]. The method has been used to successfully model the Raman spectrum of GeSe_2 , GeS_2 and SiSe_2 [43, 44].

Results for the bond-stretching modes of the $\text{GeX}_{(4-m)}\text{I}_m$ tetrahedra ($X = \text{S}$ and Se) are shown in tables 2 and 3. The frequency and Raman activity are shown for four modes for each cluster. Each mode represents a linear combination of bond stretches for the four Ge–X and Ge–I bonds in each cluster. The pattern of Raman activities is very similar for all of the clusters in the Ge–Se–I family. This is so because the Ge–Se and Ge–I component bond stretches are relatively similar. Note, for example, that the symmetric stretch modes in the $m = 0$ and 4 tetrahedra are close, at 201 and 159 cm^{-1} , respectively. Thus, the mixed Ge–Se–I tetrahedra represent only a relatively minor perturbation of the GeSe_4 tetrahedron, and the vibrational eigenvectors and the Raman strengths are therefore similar in all the clusters.

The situation is quite different in the Ge–S–I series. The Ge–S and Ge–I component bonds are very different vibrationally, as can be seen by the large difference in the $m = 0$ and 4 stretch modes, 343 and 159 cm^{-1} , respectively. In this case, the mixed clusters are strong perturbations of the GeS_4 tetrahedron. One result of this is that the Raman intensity in the mixed clusters is split between two modes, instead of being concentrated in only a single mode. Generally, strong Raman activity is associated with in-phase combinations of bond stretches, or breathing modes. In the mixed Ge–S–I clusters ($m = 1$ –3), one can think separately of symmetric combinations

Table 2. Predicted Raman activity of various local tetrahedral structures (m), mode frequencies (ω) and Raman cross-section (σ) in ternary $\text{Ge}_{0.25}\text{Se}_{0.75-y}\text{I}_y$ glasses.

Ge–Se–I				
m	Symmetric		Asymmetric	
	ω (cm^{-1})	σ	ω (cm^{-1})	σ
0	201	31.2	310	4.7
			285	4.7
			285	4.7
1	186	28.2	291	5.6
			262	7.5
2	174	26.9	249	3.8
			290	6.4
3	166	27.4	257	4.2
			299	0.7
4	159	27.6	261	4.1
			261	4.1
			261	4.1

Table 3. Predicted Raman activity of various local tetrahedral structures (m), mode frequencies (ω) and Raman cross-section (σ) in ternary $\text{Ge}_{0.25}\text{S}_{0.75-y}\text{I}_y$ glasses.

Ge–S–I				
m	Symmetric		Asymmetric	
	ω (cm^{-1})	σ	ω (cm^{-1})	σ
0	347	49.5	402	6.2
			412	8.6
			412	8.6
1	226	13.5	398	8.4
			358	38.7
2	202	23.6	249	3.1
			387	20.7
3	183	26.4	260	3.7
			400	14.7
4	159	27.6	261	4.1
			261	4.1
			261	4.1

of the Ge–S and Ge–I bonds. These symmetric components are then mixed in either in-phase or out-of-phase combinations to create the overall cluster normal modes, and both have significant Raman activity. The other modes in these clusters are built of asymmetric combinations of the Ge–S and Ge–I bonds, respectively.

In figure 5, we use the data in tables 2 and 3 to identify the experimentally observed Raman modes. We distinguish between symmetric (s) and asymmetric (a) modes as described above. The agreement in the observed and predicted positions is excellent for both Ge–S–I and Ge–Se–I systems.

4. Discussion

4.1. Binary $\text{Ge}_x\text{Se}_{1-x}$ glasses: onset of rigidity, intermediate phase and molecular structure

The base $\text{Ge}_x\text{Se}_{1-x}$ glasses have been extensively examined [45] over the years in a variety of experiments including neutron structure factors [46], x-ray structure factors [47, 48], Raman scattering, ^{129}I Mossbauer spectroscopy, ^{119}Sn Mossbauer spectroscopy and modulated DSC [49]. The picture of glass structure suggested by these results is that Ge as an additive in a Se glass serves to progressively cross-link chains of Se_n by acquiring a locally fourfold coordination. With increasing Ge concentration, the corner sharing (CS) GeSe_4 tetrahedra separated by extended Se_n chains come closer together as the chain-lengths reduce, and eventually are bridged by a Se atom. Near $x \sim 0.10$, edge sharing (ES) GeSe_2 units emerge, in which a pair of GeSe_4 tetrahedra can share an edge in addition to a corner. At $x \sim 0.30$, ethane-like Ge_2Se_6 units (homopolar Ge–Ge bonds) first emerge [49, 50] as noted in Raman scattering and ^{119}Sn Mossbauer spectroscopy experiments. Variations of $T_g(x)$ (figure 2) can be understood quantitatively in terms of SAT (section 3.3) in the $0 < x < 0.20$ range as was mentioned earlier. It is in this respect that SAT has proved to be a powerful tool to understand the correlation between T_g and network structure of glasses. Glass structure probes such as Raman scattering [49], NMR [51] and Mossbauer effect [49] are powerful in identifying local structures. However, these probes alone cannot tell if local structures form in the same backbone (fully polymerized) or whether they form part of separate backbones (nanoscale phase separated). In the latter respect, important insights into network connectivity have emerged from variations of T_g as a function of chemical composition when these are correlated with site distributions inferred from local probes. These correlations have permitted one to identify if glassy networks are fully polymerized or nanoscale phase separated [52] into more than one type of backbone. The sharp reduction in the slope, dT_g/dx , at $x > 0.31$ when Ge–Ge bonds are first detected in Raman and Mossbauer spectroscopic measurements unequivocally suggests that ethane-like units do *not* form part of the Ge–Se backbone, but nano-scale phase separate (NSPS) as discussed elsewhere [49, 53].

The non-reversing enthalpy (ΔH_{nr}) associated with T_g provides a measure of the configurational entropy change [22] between a glass and its melt. The vanishing of ΔH_{nr} in the $x_c(1) = 0.20 < x < x_c(2) = 0.25$ range or the $r_c(1) = 2.4 < x < r_c(2) = 2.5$ range shows that glasses in this range are configurationally quite close to corresponding melts [22, 54]. Changes in bonding configurations due to structural arrest of the liquid to form a glass are thus minimal for glasses in the IP. It is for this reason that the glass forming tendency is optimized in the reversibility window, and one can realize glasses even when melts are air cooled or cooled even slower (1°C min^{-1}). Glass compositions at $x < x_c(1) = 0.20$ belong to a flexible phase, while compositions at $x > x_c(2) = 0.25$ to a stressed–rigid phase. In the former floppy modes steadily increase, while in the latter redundant bonds steadily proliferate as one goes away from the reversibility window.

Raman pressure experiments on glasses reveal that vibrational modes will, in general, blue-shift, but only once the external pressure (P) exceeds a critical value, $P = P_c$. The pressure P_c is generally taken as a measure of network stress that must be overcome before an external pressure can squeeze bonds. Recent Raman pressure measurements [11] on binary $\text{Ge}_x\text{Se}_{1-x}$ glasses have revealed that P_c vanishes for IP compositions and increases steadily both at $x > 0.25$ and $x < 0.20$. These results serve to demonstrate the stress-free nature of the IP, and the stressed nature of glasses both in the floppy and stressed–rigid phases. The increase in ΔH_{nr} for both floppy and stressed–rigid glasses as one goes away from the IP correlates well with the compositional trends in P_c . The robustness of structure for glasses in the IP is

signalled by the vanishing of ΔH_{nr} , while the fragility of glass structure for glasses outside the IP by the increasing magnitude of ΔH_{nr} as one goes away from the IP. It is, indeed, comforting to see that these ideas on robustness of network structure emerging from investigations on the glassy state ($T < T_g$) correlate [16, 55] rather well with existing notion of the fragile–strong classification [56, 57] of corresponding melts based on the activation energies of viscosity of melts [20]. To summarize, IP glasses give rise to strong melts [20] while floppy and stressed–rigid glasses to fragile melts.

What can we say about the structure and width of the intermediate phase in binary Ge–Se glasses? There are two isostatic local structures populated in these binary glasses and these include CS GeSe_4 tetrahedra ($r = 2.40$) bridged across Se–Se dimers and ES $\text{Ge}(\text{Se}_{1/2})_4$ ($r = 2.67$). The observed reversibility window spans an r -range of 2.40–2.52, not quite as wide as these isostatic local structures would suggest, but at least qualitatively in the right direction. New insights into the width of the intermediate phase in Ge–Se glasses have emerged [58] from the size increasing cluster agglomeration (SICA) approach. Specifically, it has been shown that medium range order elements such as ES tetrahedra that are weakly stressed–rigid are responsible for the width of the IP in binary Ge–Se glasses. The narrow IP observed in the present chalcogenide glasses will be discussed in section 4.2.4.

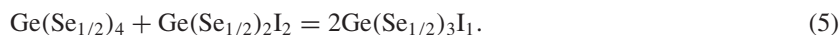
4.2. $\text{Ge}_{1/4}\text{Se}_{3/4-y}\text{I}_y$ glasses: molecular structure, variations in T_g and elastic phases

4.2.1. Molecular structure. The Pauling electronegativities [59] of Ge, Se and I are respectively 1.8, 2.55 and 2.66. One expects iodine to covalently bond with Ge rather than Se and to maximize charge transfer effects. The parent chalcogenide network glass will be steadily scissioned as Se bridges are replaced by terminal iodine atoms. Thus, as I for Se replacement proceeds, one expects fourfold-coordinated $\text{Ge}(\text{Se}_{1/2})_4$ units ($m = 0$) to be steadily transformed into mixed $\text{Ge}(\text{Se}_{1/2})_{4-m}\text{I}_m$ tetrahedral units; in the first step $m = 1$ units will form from $m = 0$ units, then $m = 2$ units from $m = 1$ units and so on, till finally $m = 4$ units result. In Raman scattering (figure 5), the narrow modes in the $150 \text{ cm}^{-1} < \nu < 200 \text{ cm}^{-1}$ range that steadily grow in scattering strength with increasing iodine concentration are identified with these mixed tetrahedral units. Support for the identification comes from the first principles cluster calculations of the Raman modes of these units as discussed earlier in section 3.4. These Raman scattering results through the distribution of m -units provide details of glass structure that are unprecedented for their details. The combinatorial predictions (section 3.3) serve as an important baseline variation that reflects what one might expect for these m -unit concentrations if iodine were to *randomly* substitute for available Se sites in the base glass network.

The richness of m -unit variations (figure 8) serves a good starting point to discuss the molecular structure of the present chalcogenide glass. Several observations become transparent. First, at low $y (< 1/6)$, we note that variations in m -unit populations, $N_m(y)/N$, deviate significantly from the combinatorial predictions. In particular, the population of $m = 0$ units is found to be systematically lower, while those of $m = 1$ units to be systematically higher than the combinatorial predictions. Second, one observes a *sharp* step in $N_1(y)/N$ and in $N_0(y)/N$ in the narrow range $0.155(2) < y < 0.163(2)$. The step is absent in corresponding sulfide glasses [13]. Furthermore, we find that the location of this step in y -space coincides with the reversibility window as shown in figure 9(a). These results undoubtedly suggest that the step is a signature of the intermediate phase (IP), a point we discuss further in section 4.2.4.

Third, as y exceeds $y_c(1) = 0.155(2)$ other changes in glass structure occur; the population of $m = 2$ units, $N_2(y)/N$, decreases more rapidly than predicted by combinatorics. It appears that $m = 0$ and 2 units coalesce to produce twice as many $m = 1$ units by a reaction that can

be summarized as follows:



The iodine conserving transformation described by equation (5) above probably contributes to the sharp step in $N_1(y)/N$ across the reversibility window, a process that underlies network reconfiguration to minimize stress, i.e. self-organize.

Fourth, as $y > y_c(2) = 0.163(2)$, the slack in the population of $m = 2$ units between the observed and combinatorial predictions is taken up by the populations of the $m = 3$ and 4 units, which are observed to exceed the combinatorial values. The result is observed in both the ternary selenide (figure 8) and ternary sulfide [13] glasses, but with a difference (see below). The $m = 2$ units have two iodine near neighbours of Ge and are substantially stressed, and it is energetically favourable for the $m = 2$ units to combine within limits of available iodine to form terminal GeI_3S tetrahedral units ($m = 3$) and isolated GeI_4 molecules ($m = 4$). The GeI_4 molecules decouple from the backbone as they are bonded by weaker van der Waals forces to the rest of the network. In the ternary sulfide glasses, starting with an iodine concentration $y > y_c(1)$, the underlying networks show a propensity to nanoscale phase separate, as evidenced [13] by the rapid growth of the $m = 3$ and 4 units. The tendency is less pronounced in the present ternary selenide glasses (figure 8), which are qualitatively more polymerized than their sulfide counterparts.

These features of glass structure stem from the larger size of the halogen additive (iodine) in relation to the chalcogen (S or Se) substituents, and it is likely that these effects will be suppressed in chalcohalide glasses containing smaller sized halogen atoms such as Cl and Br. A broad consequence of the backbone fragmentation is that underlying network connectivities plummet with increasing iodine concentration, and the effect is directly reflected in the glass transition temperatures as will be discussed next.

4.2.2. Variations of T_g with glass composition. We had commented on the usefulness of SAT as a method to understand compositional trends of T_g in the present ternary glasses in section 3.3. The slope equation (4), deduced from a minimalist approach, does *not* accurately describe the compositional trends in $T_g(y)$ in the ternary chalcohalide glasses even at low iodine concentrations ($y < 0.05$). Furthermore, the observed variations of T_g (figure 3) are strongly dependent on the nature of the chalcogen involved, sulfur or selenium, a situation that is in sharp contrast to the behaviour observed in binary $\text{Ge}_x(\text{S or Se})_{1-x}$ glasses [9].

In the present ternary glasses, there are four possible LSs, $m = 0, 1, 2$ and 3, populated in the glasses, and the distribution of iodine is strictly not random in these LSs. The agglomeration processes rapidly increase as the count of LSs increases and render the calculations rather intensive. We have carried out SAT calculations [39] taking into account structural correlations between $m = 0$ and 1 units, between pairs of $m = 1$ units and between $m = 0$ and 2 units. From these detailed calculations, we can project the populations of the various m -units, and the expected variations in T_g for the two ternaries. Under these assumptions, the SAT predicted variations in T_g for the ternary sulfide glasses are given by the broken curves for the two ternaries in figure 3. These predictions converge to the exact result (3) when y goes to zero. Furthermore, these approximate calculations appear to capture the gist of the observed variations in glass structure including the m -unit probabilities with respect to the iodine concentration, and T_g trends in the two ternaries up to $y = 0.10$.

Within SAT, the steeper reduction of $T_g(y)$ in the ternary sulfide glasses in relation to the ternary selenide glasses (figure 3) suggests that the connectivity reduction is more pronounced because of a higher population of $m = 3$ units in the former. At $x = 0.10$, the SAT calculations show population of $m = 3$ units, $p_3 = 0.20$, in the $\text{Ge}_{1/4}\text{S}_{3/4-y}\text{I}_y$ ternary, and $p_3 = 0.29$

in the $\text{Ge}_{1/4}\text{Se}_{3/4-y}\text{I}_y$ ternary. On the other hand, this leads to an increase of the $m = 2$ unit concentrations with $p_2 = 0.06$ for the sulfide and 0.02 for the selenide glasses at y_c . These findings are broadly consistent with the measured m -unit concentrations (figure 8) at $x = 0.10$. With increasing iodine content, additional units appear ($m = 3$ and 4) that are not taken into the SAT calculations at present, and their lack undoubtedly contributes to the progressive deviation of the predicted (figure 3) from the observed $T_g(y)$ trends as y exceeds 0.10. In the experiments, populations of the $m = 4$ local structures are, again, found to be larger in the ternary sulfides than in the selenides. This leads to a deviation with respect to experiment at lower concentrations of iodine in the sulfide glasses in relation to the selenides.

With the evolution of the probabilities p_{mm} ($m = 0, 1, 2$) with iodine concentration within SAT, it is then possible to compute the number of constraints according to equation (2b), and we find that onset of rigidity, i.e. realization of the condition $n_c = 3$, appears at a lower iodine concentration in the Se-based glasses ($y_c = 0.150$) than in the S-based ones ($y_c = 0.168$). The result is consistent with the observed variations in $T_g(y)$ and the location of the reversibility windows. In particular, the window in the ternary selenides (figure 9(a)) is shifted to lower iodine concentration in relation to the one in the ternary sulfides (figure 9(b)).

In summary, the SAT approach shows that variations in glass structure through m -unit concentrations are encoded in those of T_g and the onset of rigidity or the reversibility windows. The finding provides self-consistency of the observed thermal and optical results described in this work.

4.2.3. Identification of the three elastic phases in $\text{Ge}_{1/4}\text{Se}_{3/4-y}\text{I}_y$ glasses. In estimating Lagrangian constraints, terminal or onefold coordinated atoms ($r = 1$) have to be treated differently from atoms possessing a coordination number of two or larger. Only bond-stretching constraints can be associated with terminal atoms, while both bond-stretching and bond-bending constraints are involved with atoms possessing $r = 2$ or greater. The realization led [25] to the recognition that the mean-field rigidity transition of a network containing a fraction y of terminal atoms will occur when the connectivity (r) acquires a threshold value (r_c), given by

$$r_c = 2.40 - 0.4y \quad (6a)$$

In ternary $\text{Ge}_{1/4}\text{Se}_{3/4-y}\text{I}_y$ glasses the mean coordination number becomes $2.5 - y$, and the rigid to floppy phase transition is then predicted to occur at a critical concentration $y = y_c$, given by

$$2.5 - y_c = 2.40 - 0.4y_c \quad (6b)$$

or

$$y_c = 1/6. \quad (6c)$$

The prediction of the elastic phase boundary at $y_c = 1/6$ is in reasonable agreement with the centroid of the reversibility window at $y_c = 0.159(3)$ in our MDSC experiments on $\text{Ge}_{1/4}\text{Se}_{3/4-y}\text{I}_y$ glasses (figure 9(a)). In spite of the agreement, the glass structure evolution with y is far from being a *random network structure* (see below).

The finding of reversibility windows in both $\text{Ge}_{1/4}\text{Se}_{3/4-y}\text{I}_y$ and $\text{Ge}_{1/4}\text{S}_{3/4-y}\text{I}_y$ glasses unequivocally shows that *non-mean-field effects* are manifested in their molecular structures. The global minimum in the non-reversing enthalpy $\Delta H_{nr}(y)$ (figures 9(a) and (b)) in the $y_c(1) < y < y_c(2)$ range, in analogy to the reversibility windows observed in several binary and ternary chalcogenide glasses [11], permits identification of the *three* elastic phases in the present glasses. Glasses in the $0 < y < y_c(1)$ are identified as belonging to the *stressed-rigid phase*, those in the reversibility window $y_c(1) < y < y_c(2)$ with the *intermediate phase* and those at $y > y_c(2)$ with the *floppy elastic phase*.

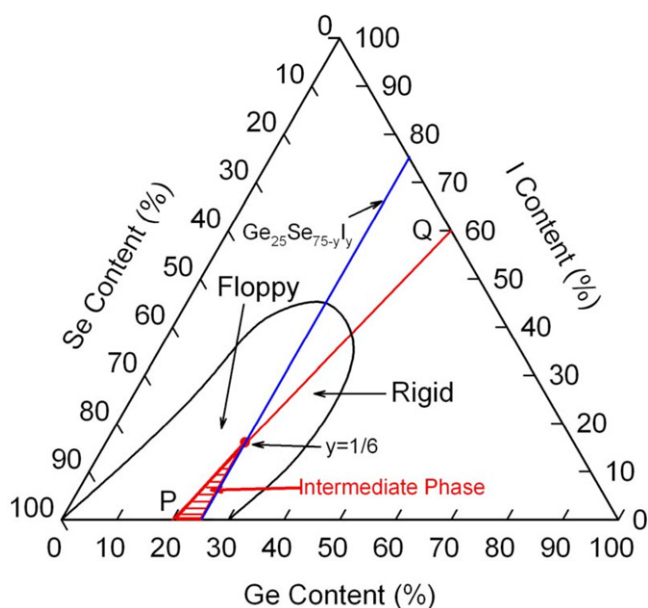


Figure 11. Glass forming region in the Ge–Se–I composition triangle taken from [60, 61]. PQ (red) represents the mean-field elastic phase boundary with compositions to the left (right) being floppy (stressed–rigid). Compositions synthesized in the present work are shown by the blue line. It intersects the phase boundary near $y \sim 1/6$. The red hatched region indicates the intermediate phase, and it is constructed using the results on binary $\text{Ge}_x\text{Se}_{1-x}$ glasses and ternary $\text{Ge}_{0.25}\text{Se}_{0.75-y}\text{I}_y$ glasses.

In the composition triangle of figure 11, we have delineated the glass forming range in the Ge–Se–I ternary from earlier work [60, 61]. The thin red line PQ defines the mean-field phase boundary between the floppy phase ($n_c < 3$) on the left and the stressed–rigid phase ($n_c > 3$) on the right of this line. The line PQ is calculated based on the premise that Ge, Se and I are respectively four-, two- and onefold coordinated, and that the isostaticity of the random network, i.e. $n_c = 3$, is satisfied along this line. In figure 11, the thick blue line labelled $\text{Ge}_{25}\text{Se}_{75-y}\text{I}_y$ represents the compositional pathway along which samples were synthesized in the present work. The IP region suggested by the available results most likely encloses a triangle (hashed marked region in figure 11) whose base is fixed by the IP in binary Ge–Se glasses [5], and whose vertex by the IP in the present experiments on Ge–Se–I ternary glasses.

What can one say about glass structure in the IP of ternary $\text{Ge}_{1/4}\text{Se}_{3/4-y}\text{I}_y$ glasses? First of all, the IP width is narrow and rather clearly defined. The sharpness of the elastic phase boundaries at $y = y_c(1)$ and at $y = y_c(2)$ is reflected in the discontinuous variations in populations of the $m = 0, 1$ and 2 units observed in Raman scattering (figures 8 and 9). The *steplike increase* in $N_1(y)/N$ at the expense of $N_0(y)/N$ in the narrow IP is strongly suggestive of cooperative processes. The underlying structure changes are driven to minimize network stress in the IP (see below).

Our experimental data reveals that *three* isostatic local structures form part of the IP ($2.245 < r < 2.236$) of $\text{Ge}_{0.25}\text{Se}_{0.75-y}\text{I}_y$ glasses. These include (i) the $m = 1$ units— $\text{Ge}(\text{Se}_{1/2})_3\text{I}_1$ ($r = 2.14$), (ii) the CS $\text{Ge}(\text{Se})_4$ units ($r = 2.40$) between Se–Se dimers and (iii) the ES $\text{Ge}(\text{Se}_{1/2})_4$ tetrahedra ($r = 2.67$) (see table 1). The IP-width narrowing is driven by conversion of the CS and ES units of the base glass into the $m = 1$ mixed tetrahedral units of the ternary glass. If only local structure (i) was populated in the ternary glasses, one would

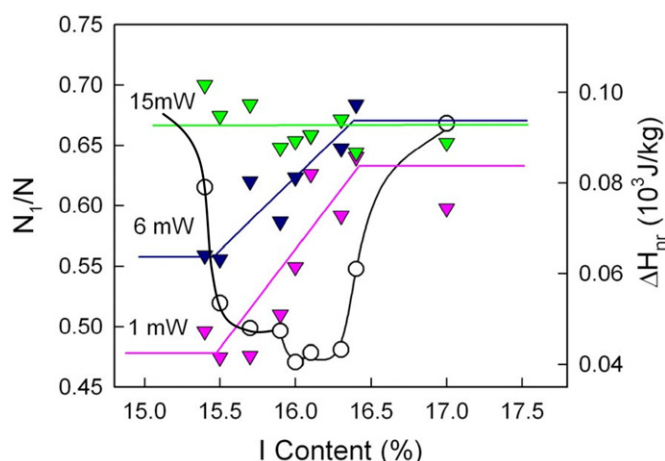


Figure 12. Variations in the concentration of $m = 1$ units deduced from micro-Raman studies undertaken as a function of exciting laser (647 nm) power in ternary $\text{Ge}_{25}\text{Se}_{75-y}\text{I}_y$ glasses. Red triangles (\blacktriangledown), $\mathcal{P} = 1$ mW; blue triangles (\blacktriangledown), $\mathcal{P} = 6$ mW; green triangles (\blacktriangledown), $\mathcal{P} = 15$ mW. The step height decreases with increasing laser power and it vanishes at $\mathcal{P} = 15$ mW. In these Raman scattering experiments samples were confined in evacuated quartz ampoules, wetting the inside surface, and the light beam was brought to a line focus on the sample surface in contact with the quartz envelope. The reversibility window, taken from figure 8, provides a guide to the intermediate phase region.

have expected the mean-field elastic phase boundary to occur near $r = 2.14$ corresponding to the stoichiometry of the $m = 1$ units. A small but finite concentration of CS GeSe_4 and ES GeSe_2 units of the base glass persist in the IP region of the ternary as revealed by the Raman lineshapes (figure 5). There is a rapid conversion of ES into CS tetrahedra in the very narrow IP as shown in figure 10. An analysis of the Raman lineshapes in the $180 \text{ cm}^{-1} < \nu < 220 \text{ cm}^{-1}$ range (figure 5) shows that the maximum in scattering strength ratio of CS to ES units of about 3.0 in the reversibility window is actually quite similar to that found in the base glass ($\text{Ge}_{25}\text{Se}_{75}$), a network that is close to being self-organized as well. Thus, the principal isostatic local structures present in the IP of the ternary glass include the $m = 1$ mixed tetrahedral units, CS GeSe_4 units and ES GeSe_2 units in decreasing order of concentration. The next step in this programme is to quantitatively understand these structure results by building models of the present ternary glasses using either by MD simulations or a SICA-based algorithm [58] and identify the elements of medium range structures that are responsible for the formation of the IP.

4.2.4. Intermediate phases in ternary $\text{Ge}_{1/4}\text{Se}_{3/4-y}\text{I}_y$ and $\text{Ge}_{1/4}\text{S}_{3/4-y}\text{I}_y$ glasses compared: role of atom size mismatch and global network stress. In this work we have identified intermediate phases (IPs) in the $\text{Ge}_{1/4}\text{Se}_{3/4-y}\text{I}_y$ ternary. The case of the ternary sulfide was discussed earlier [13]. In spite of their chemical similarity, there are glaring differences in the ways these two networks shed their stress to self-organize in the IPs. In this section we comment on the issue and will show that atomic size mismatch plays a crucial role in the way these glassy networks self-organize.

We begin by summarizing the principal findings on the IPs from the measured reversibility windows. In ternary $\text{Ge}_{1/4}\text{S}_{3/4-y}\text{I}_y$ glasses, the IP starts near $y_c(1) = 0.162(1)$ and ends near $y_c(2) = 0.167(1)$, leading to a width $\Delta r = 0.005(2)$; the window is deep at its mid-point,

i.e. $\Delta H_{\text{nr}}(y) \sim 0$ near $y = 0.164(1)$, suggesting that the IP is almost completely stress free at this composition, and its shape is almost a symmetric Gaussian. To the best of our knowledge, this is the narrowest IP reported in any glass system to date. In ternary $\text{Ge}_{1/4}\text{Se}_{3/4-y}\text{I}_y$ glasses, the IP starts near $y_c(1) = 0.155(1)$ and ends near $y_c(2) = 0.164(1)$, leading to a width $\Delta r = 0.009(2)$; the window is wider but also shallower, i.e. $\Delta H_{\text{nr}}(y) \sim 0.05 \text{ kJ kg}^{-1}$, suggesting that the IP is not quite stress free. Furthermore, the IP possesses rather well defined phase boundaries to display a square-well-like shape (figure 9).

Understanding global stress in glassy networks has been elusive but not because of the lack of trying [12]. It has already been established that the connectivity of a glass network plays a vital role in determining stress. In multi-component glasses network stress is also determined by atomic size distribution. It will be useful to recall here the dielectric covalent radii [62] of Se, $r_{\text{cov}} = 1.225 \text{ \AA}$, of Ge, $r_{\text{cov}} = 1.225 \text{ \AA}$, of S, $r_{\text{cov}} = 1.127 \text{ \AA}$, and of I, $r_{\text{cov}}(\text{I}) = 1.405 \text{ \AA}$. In the case of binary $\text{Ge}_x\text{Se}_{1-x}$ glasses, one has a network composed of two types of atoms (Ge, Se) that have the *same* size. In this system, network stress can be expected to be *homogeneously* distributed around both the Ge and Se atoms, and the local stress around Ge atoms to be a good representation of the global network stress in the glasses. In Raman scattering experiments, the shift of A_1 mode frequency of GeSe_4 tetrahedra with external pressure measures the *local* stress around Ge atoms, and it is actually a good measure of *global* network stress [11]. As shown earlier the mode shifts only when the external P exceeds a critical value, P_c , and P_c provides a good measure of *global* network stress. The vanishing of P_c in the reversibility window, and its steady increase in both stressed-rigid and floppy glasses as one goes away from the window region, are features we have commented upon earlier [11]. On the other hand, such Raman scattering measurements on binary Ge–S glasses reveal the behaviour of P_c to be quite different [11]. The atomic size difference between Ge and S leads global stress to be inhomogeneously distributed, with the consequence that the *local* stress around Ge atoms (probed in Raman pressure experiments) is *no longer* a good measure of *global network* stress in the sulfide glassy networks.

Let us now turn to the case of the present ternary $\text{Ge}_{0.25}\text{Se}_{0.75-y}\text{I}_y$ glasses. Here one expects *local* packing stresses around Ge atoms to accumulate as the oversized iodine replaces Se, and a part of this *local* stress is offset because of loss of network connectedness as terminal iodine atoms replace bridging Se atoms. A qualitatively similar behaviour is expected in ternary $\text{Ge}_{0.25}\text{S}_{0.75-y}\text{I}_y$ glasses. In our Raman experiments, the A_1 mode frequencies of the Ge-centred $m = 0$ units in both glass systems are found to increase as y increases in somewhat parallel fashion. These results underscore the growth of *local* stress around Ge atoms in respective glasses.

There is, however, a sharp difference when it comes to estimating *global stress* in these glasses. In ternary $\text{Ge}_{0.25}\text{Se}_{0.75-y}\text{I}_y$ glasses, I for Se replacement invariably leads to a pronounced increase of *global stress* in the glassy networks because I atoms (1.405 \AA) have a bigger size than Se atoms (1.225 \AA). On the other hand, in ternary $\text{Ge}_{0.25}\text{S}_{0.75-y}\text{I}_y$ glasses, one can expect some stress compensation to occur as the larger-sized I anion (1.405 \AA) replaces the smaller-sized S anion (1.127 \AA). Atomic volume considerations alone suggest that as much as 35 at.% of S can be replaced by I before one achieves anion-size parity with the case of Se. Thus, *global* network stress in ternary $\text{Ge}_{1/4}\text{S}_{3/4-y}\text{I}_y$ glasses, in general, will always be much lower than in corresponding selenide glasses.

These considerations on atomic size distribution apparently play an important role in determining the observed variations of m -unit concentrations of figure 8. Thus, m -unit concentrations closely track the combinatorial predictions in the ternary sulfides [13], largely because *global network stress* does not accumulate due to an anion size compensation effect. On the other hand, in the ternary selenides, the transfer of population from $m = 0$ to 1 mixed

units occurs more rapidly in the $0 < y < y_c(1)$ range than the combinatorial predictions. Furthermore, the conversion proceeds at an *extremely rapid* rate in the reversibility window, a result that is completely unexpected within the combinatorial predictions. These variations are a response of the glass network to the accumulation of *global stress* as I for Se substitution proceeds. The glass network offsets the accumulation of global network stress by reorganizing and forming the isostatic $m = 1$ units at the expense of the stressed–rigid $m = 0$ ones. Even with these profound structural changes, it appears that the network stress in the IP never reaches the same low levels as found in the corresponding sulfides. We have already noted that the ΔH_{nr} term in the reversibility window of the ternary selenides never reaches zero (figure 8), as it does in the ternary sulfides.

In summary, it appears that ternary $\text{Ge}_{1/4}\text{S}_{3/4-y}\text{I}_y$ glasses self-organize over a very narrow iodine concentration range to form an almost completely stress-free backbone. The narrowness of the IP width results because of the tendency of these glasses to nanoscale phase separate, i.e. growth of $m = 3$ and 4 units already near the IP composition. On the other hand, the corresponding ternary selenide glasses self-organize over a larger iodine concentration because of their tendency to qualitatively polymerize. In the ternary selenides, $m = 3$ and 4 units also occur but their appearance is shifted to a higher iodine concentration in relation to the ternary sulfides. The IP of ternary selenide glasses appears to have well defined phase boundaries, although the backbone within the IP is not as completely stress free as in their sulfide counterparts.

4.3. Light induced collapse of intermediate phases in glassy networks

Photostructural transformations in glassy networks have displayed a richness of phenomenology [63–67] that continues to be a subject of interest from both a basic as well as applications point of view. The latter interest derives from the fact that chalcogenides in their glassy or amorphous form have found commercial use in several technologies including information storage [68], memory devices [69], and mid-IR sources and imaging [70, 71]. Our basic understanding of these light induced effects continues to evolve. The metastability of lone-pair electron bonding configurations associated with the chalcogens has often been identified [72, 73] with the propensity of photo-structural effects displayed by glasses. In particular, the metastable local bonding configurations taken on by chalcogens in the glassy state have been modelled [63, 64] and discussed in relation to the richness of photostructural effects displayed by these materials in several reviews on the subject.

The central role played by the connectivity of a network in photostructural transformations of chalcogenide glasses was recognized more recently [74, 75] in the field. The identification of elastic phases in glasses has facilitated understanding the role of networks in this context. In particular, the giant softening [74] of the longitudinal acoustic mode in $\text{Ge}_x\text{Se}_{1-x}$ glasses near the mean-field rigidity transition in Brillouin scattering measurements has underscored the importance of network stress in facilitating photostructural transformations. Raman scattering measurements performed as a function of exciting light power, on the same binary glass system, have highlighted the collapse of the IP [5]. The IP of binary $\text{Ge}_x\text{Se}_{1-x}$ glasses is readily observed when the exciting light power density, \mathcal{P} , is kept low ($1 \text{ mW}/(50 \mu\text{m})^2$), as in the macro-Raman scattering experiments. On the other hand, the IP is found to collapse [5] when light power density \mathcal{P} is high ($1 \text{ mW}/(1 \mu\text{m})^2$), as in the micro-Raman experiments. Both Brillouin and Raman scattering experiments, taken together, serve to show that rapid switching of nearest-neighbour covalent bonds by exciting light is qualitatively suppressed for glass compositions outside the IP, underscoring in no uncertain terms that the interaction of light with a glassy network is promoted (hindered) by the absence (presence) of network stress.

The present Raman scattering results (figure 12) on ternary $\text{Ge}_{1/4}\text{Se}_{3/4-y}\text{I}_y$ glasses performed as a function of light power (\mathcal{P}) in the $1 \text{ mW} < \mathcal{P} < 15 \text{ mW}$ range reveal systematic trends in $N_1(y)/N$; the step is readily observed at low power densities, and it steadily decreases in height and is finally lost as the power density \mathcal{P} increases to 15 mW. Our interpretation of these results is that at $\mathcal{P} = 15 \text{ mW}$ the self-organized backbone completely transforms into a random network. The underlying photostructural transformations, following the work of H. Fritzsche [72, 73], can be roughly described as follows. Near-bandgap light serves to produce electron–hole pairs, leading to the formation of excitons. Thereafter, local structural rearrangements follow and excitons undergo non-radiative recombination. The underlying switching of chemical bonds is rapid and extensive as the light power density \mathcal{P} increases and leads to a state of higher free energy, in which the medium range structure changes. The self-organized network observed at low power densities reversibly transforms to a random network state at high power densities. The random network state so formed is a light-pumped dynamic state of the glass. Once the exciting light is removed, the network returns to its pristine, self-organized, low free-energy state.

The present observation is reminiscent of the previous result [5] on binary $\text{Ge}_x\text{Se}_{1-x}$ glasses, where in Raman scattering the IP could be completely collapsed by increasing the exciting light power density. Taken together, both these experiments illustrate that the self-organized state is a stress-free and low energy state of glasses. The facile transfer of light energy to covalent bonds leads to a melting of the glass that is optically driven, i.e. photomelting, and it is to be contrasted to melting achieved by heating a glass sample to its glass transition temperature.

5. Concluding remarks

A measurement of the reversibility window in ternary $\text{Ge}_{1/4}\text{Se}_{3/4-y}\text{I}_y$ glasses reveals the intermediate phase (IP) to reside in the $0.155 < y < 0.164$ range or $2.236 < r < 2.245$. The IP in the parent binary $\text{Ge}_x\text{Se}_{1-x}$ glass was shown earlier to reside in the $0.20 < x < 0.25$ range or $2.40 < r < 2.52$ range. Thus, the IP width of the binary glass of $\Delta r = 0.10(2)$ collapses by a factor of 10 to $\Delta r = 0.009(2)$ in the ternary. The result broadly follows from terminal I atoms cutting characteristic Ge–Se rings of the base $\text{Ge}_{25}\text{Se}_{75}$ glass where isostatic rigidity is nucleated. The IP in the present ternary $\text{Ge}_{1/4}\text{Se}_{3/4-y}\text{I}_y$ glasses ($\Delta r = 0.009(2)$) is wider than in corresponding sulfide glasses ($\Delta r = 0.005(2)$). In the ternary selenides, Raman scattering reveals a spectacular first-order structural reorganization in the IP with the concentration of the mixed tetrahedral unit $\text{Ge}(\text{Se}_{1/2})_3\text{I}$ ($m = 1$ units) increasing linearly with iodine concentration y to offset strain accumulated due to I for Se replacement. Such a structural reorganization is not observed in corresponding ternary sulfide glasses, we suppose because of a *size compensation effect* as the oversized iodine replaces the undersized sulfur anion. Finally, the sharp step in the concentration of $m = 1$ units observed in the narrow IP of the ternary selenide glasses can be steadily erased by increasing the laser power used to excite the Raman scattering, an observation that constitutes evidence for photomelting of the self-organized IP to form a random network. Two recent publications on intermediate phases in network glasses have just appeared online. One of these [76] provides a historical perspective of the field including the role of theory and experiment in understanding the nature of the phase. The other contribution [77] provides evidence for the intermediate phase in thin-film gate dielectrics, which are thought to be central to the functioning of three-terminal devices.

Acknowledgments

We have benefited from discussions with Professor J C Phillips, Professor Bernard Goodman and Professor Darl H McDaniel during the course of this work. This work is supported in part by NSF grants DMR-01-01808 and 04-56472.

References

- [1] Dittmar V G and Schaefer H 1976 *Acta Crystallogr. B* **32** 2726
- [2] Dittmar V G and Schaefer H 1976 *Acta Crystallogr. B* **32** 1188
- [3] Dittmar V G and Schaefer H 1975 *Acta Crystallogr. B* **31** 2060
- [4] Phillips J C 1979 *J. Non-Cryst. Solids* **34** 153–81
- [5] Boolchand P, Feng X and Bresser W J 2001 *J. Non-Cryst. Solids* **293** 348–56
- [6] Kalampounias A G, Andrikopoulos K S and Yannopoulos S N 2003 *J. Chem. Phys.* **119** 7543–53
- [7] Vempati U and Boolchand P 2004 *J. Phys.: Condens. Matter* **16** S5121–38
- [8] Qu T and Boolchand P 2005 *Phil. Mag.* **85** 875–84
- [9] Feng X W, Bresser W J and Boolchand P 1997 *Phys. Rev. Lett.* **78** 4422–5
- [10] Vempati U K 2003 *MS Thesis* University of Cincinnati
- [11] Wang F, Mamedov S, Boolchand P, Goodman B and Chandrasekhar M 2005 *Phys. Rev. B* **71** 174201
- [12] Alexander S 1998 *Phys. Rep.* **296** 65–236
- [13] Wang Y, Wells J, Georgiev D G, Boolchand P, Jackson K and Micoulaut M 2001 *Phys. Rev. Lett.* **87** 185503
- [14] Selvanathan D, Bresser W J and Boolchand P 2000 *Phys. Rev. B* **61** 15061–76
- [15] Selvanathan D, Bresser W J, Boolchand P and Goodman B 1999 *Solid State Commun.* **111** 619–24
- [16] Boolchand P, Georgiev D G and Goodman B 2001 *J. Optoelectron. Adv. Mater.* **3** 703–20
- [17] Micoulaut M 2006 *Phys. Rev. B* **74** 184208–5
- [18] Barre J, Bishop A R, Lookman T and Saxena A 2005 *Phys. Rev. Lett.* **94** 208701
- [19] Thorpe M F, Jacobs D J, Chubynsky M V and Phillips J C 2000 *J. Non-Cryst. Solids* **266** 859–66
- [20] Boolchand P, Lucovsky G, Phillips J C and Thorpe M F 2005 *Phil. Mag.* **85** 3823–38
- [21] *Modulated DSC Compendium, Reprint #TA 210* 1997 T.A. Instruments, Inc, New Castle, DE
<http://www.tainstruments.com>
- [22] Boolchand P, Georgiev D G and Micoulaut M 2002 *J. Optoelectron. Adv. Mater.* **4** 823–36
- [23] Georgiev D G, Boolchand P and Micoulaut M 2000 *Phys. Rev. B* **62** R9228–31
- [24] Thorpe M F 1983 *J. Non-Cryst. Solids* **57** 355–70
- [25] Boolchand P and Thorpe M F 1994 *Phys. Rev. B* **50** 10366–8
- [26] Mitkova M and Boolchand P 1998 *J. Non-Cryst. Solids* **240** 1–21
- [27] Tanaka K 1985 *Solid State Commun.* **54** 867–9
- [28] Kauzmann W 1948 *Chem. Rev.* **43** 219–56
- [29] Tichy L and Ticha H 1994 *Mater. Lett.* **21** 313–9
- [30] Kerner R and Micoulaut M 1997 *J. Non-Cryst. Solids* **210** 298–305
- [31] Micoulaut M 1998 *Eur. Phys. J. B* **1** 277–94
- [32] Sarrach D J, de Neufville J P and Haworth W L 1976 *J. Non-Cryst. Solids* **22** 245–67
- [33] Norban B, Pershing D, Enzweiler R N, Boolchand P, Griffiths J E and Phillips J C 1987 *Phys. Rev. B* **36** 8109–14
- [34] Naumis G G 2006 *Phys. Rev. B* **73** 172202–4
- [35] Lindemann F A 1910 *Phys. Z.* **11** 609–12
- [36] Phillips W A, Buchenau U, Nücker N, Dianoux A J and Petry W 1989 *Phys. Rev. Lett.* **63** 2381
- [37] Buchenau U and Zorn R 1992 *Europhys. Lett.* **18** 523
- [38] Vaills Y, Qu T, Micoulaut M, Chaimbault F and Boolchand P 2005 *J. Phys.: Condens. Matter* **17** 4889–96
- [39] Micoulaut M 2001 *Phase Transition and Self-organization in Electronic and Molecular Networks* ed J C Phillips and M F Thorpe (New York: Kluwer Academic/Plenum) p 143
- [40] Pederson M R and Jackson K A 1990 *Phys. Rev. B* **41** 7453
- [41] Briley A, Pederson M R, Jackson K A, Patton D C and Porezag D V 1998 *Phys. Rev. B* **58** 1786
- [42] Porezag D and Pederson M R 1996 *Phys. Rev. B* **54** 7830
- [43] Jackson K, Briley A, Grossman S, Porezag D V and Pederson M R 1999 *Phys. Rev. B* **60** R14985–9
- [44] Jackson K and Grossman S 2001 *Phys. Rev. B* **65** 012206
- [45] Boolchand P, Chen P, Jin M, Goodman B and Bresser W J 2007 *Physica* **389** 18–28
- [46] Petri I, Salmon P S and Fischer H E 2000 *Phys. Rev. Lett.* **84** 2413–6
- [47] Wang Y, Ohata E, Hosokawa S, Sakurai M and Matsubara E 2004 *J. Non-Cryst. Solids* **337** 54–61
- [48] Sharma D, Sampath S, Lalla N P and Awasthi A M 2005 *Physica B* **357** 290–8
- [49] Boolchand P and Bresser W J 2000 *Phil. Mag.* **80** 1757–72
- [50] Lucovsky G, Nemanich R J and Galeener F L 1977 *Proc. 7th Int. Conf. Amorphous and Liquid Semiconductors (ICLS, University of Edinburgh, 1977)* ed W E Spear p 130
- [51] Bureau B, Troles J, Le Floch M, Smektala F and Lucas J 2003 *J. Non-Cryst. Solids* **326** 58–63
- [52] Boolchand P, Georgiev D G, Qu T, Wang F, Cai L C and Chakravarty S 2002 *C. R. Chim.* **5** 713–24
- [53] Boolchand P 2000 *Asian J. Phys.* **9** 709

- [54] Boolchand P 2006 *Chalcogenide Lett.* **3** 29
- [55] Wang Y, Boolchand P and Micoulaut M 2000 *Europhys. Lett.* **52** 633–9
- [56] Williams M L, Landel R F and Ferry J D 1955 *J. Am. Chem. Soc.* **77** 3701–7
- [57] Angell C A 1988 *J. Non-Cryst. Solids* **102** 205–21
- [58] Micoulaut M and Phillips J C 2003 *Phys. Rev. B* **67** 104204–9
- [59] Pauling L 1960 *The Nature of the Chemical Bond* (Ithaca, NY: Cornell University)
- [60] Koudelka L and Pisarcik M 1989 *J. Non-Cryst. Solids* **113** 239–45
- [61] Koudelka L 1998 private communication
- [62] Phillips J C 1973 *Bonds and Bands in Semiconductors* (New York: Academic)
- [63] Shimakawa K and Ganjoo A 2001 *J. Optoelectron. Adv. Mater.* **3** 167–76
- [64] Shimakawa K, Kolobov A and Elliott S R 1995 *Adv. Phys.* **44** 475–588
- [65] Hisakuni H and Tanaka K 1995 *Science* **270** 974–5
- [66] Chopra K L, Harshvardhan K S, Rajagopalan S and Malhotra L K 1981 *Solid State Commun.* **40** 387–90
- [67] Boolchand P, Bresser W J and Chopra K L 1999 *Bull. Am. Phys. Soc.* **44** 1434
- [68] Ohta T 2001 *J. Optoelectron. Adv. Mater.* **3** 609–26
- [69] Kozicki M N and West W C 1999 *US Patent Specification* 5896312
- [70] Sanghera J S, Shaw L B and Aggarwal I D 2002 *C. R. Chim.* **5** 873–83
- [71] Sanghera J S and Aggarwal I D 1999 *J. Non-Cryst. Solids* **257** 6–16
- [72] Fritzsche H 1996 *Solid State Commun.* **99** 153–5
- [73] Fritzsche H 2000 *Insulating and Semiconducting Glasses* ed P Boolchand (Singapore: World Scientific) pp 653–90
- [74] Gump J, Finkler I, Xia H, Sooryakumar R, Bresser W J and Boolchand P 2004 *Phys. Rev. Lett.* **92** 245501
- [75] Wang F and Boolchand P 2004 *Non-Crystalline Materials for Optoelectronics* ed G Lucovsky and M Popescu (Romania: INOE) pp 15–41
- [76] Micoulaut M and Phillips J C 2007 *J. Non-Cryst. Solids* at press
- [77] Lucovsky G, Baker D A, Paesler M A and Phillips J C 2007 *J. Non-Cryst. Solids* at press